Biomaterials 31 (2010) 8198–8209

Contents lists available at ScienceDirect

Biomaterials

journal homepage: www.elsevier.com/locate/biomaterials

Endothelial cells dysfunction induced by silica nanoparticles through oxidative stress via JNK/P53 and NF-κB pathways

Xin Liu, Jiao Sun*

Shanghai Biomaterials Research & Testing Center, Shanghai Key Laboratory of Stomatology, Ninth People's Hospital, Shanghai Jiaotong University School of Medicine, No. 427, Ju-men Road, Shanghai 200023, China

ARTICLE INFO

Article history:
Received 24 April 2010
Accepted 20 July 2010
Available online 19 August 2010

Keywords:
Silica nanoparticles
Human umbilical vein endothelial cells (HUVECs)
Oxidative stress
Apoptosis
Inflammation

ABSTRACT

Drug carriers are generally introduced into the body intravenously and directly exposed to endothelial cells. Silica nanoparticles could be promising delivery vehicles for drug targeting or gene therapy. However, few studies have been undertaken to determine the biological behavior of silica nanoparticles on endothelial cells. Here we measured reactive oxygen species (ROS) generation, apoptosis and necrosis, proinflammatory and prothrombic properties and the levels of the apoptotic signaling proteins and the transcription factors in human umbilical vein endothelial cells (HUVECs) after exposure to silica nanoparticles of different concentrations (25, 50, 100, and 200 μg/mL) for 24 h. The results showed that silica nanoparticles, ranging from 50 μg/mL to 200 μg/mL, markedly induced ROS production, mitochondrial depolarization and apoptosis in HUVECs. At the highest concentration, the necrotic rate, LDH leakage, the expression of CD54 and CD62E, and the release of TF, IL-6, IL-8 and MCP-1 were significantly increased. Silica nanoparticles also activated c-Jun N-terminal kinase (JNK), c-Jun, p53, caspase-3 and NF-κB, increased Bax expression and suppressed Bcl-2 protein. Moreover, inhibition of ROS attenuated silica nanoparticles-induced apoptosis and inflammation and the activation of JNK, c-Jun, p53 and NF-κB. In summary, our findings demonstrated that silica nanoparticles could induce dysfunction of endothelial cells through oxidative stress via JNK, p53 and NF-κB pathways, suggesting that exposure to silica nanoparticles may be a significant risk for the development of cardiovascular diseases such as atherosclerosis and thrombus.

© 2010 Elsevier Ltd. All rights reserved.

1. Introduction

Nanomaterials, defined as particles with diameters of less than 100 nm, have been rapidly applied in technical and medicinal fields due to their unique physiochemical properties and tunable characteristics. One of the most important members of this class of materials is silica nanoparticles, which have been found extensive applications in biomedical and biotechnological fields, such as drug carrier, gene therapy, and molecular imaging [1–3]. Thus, possible health impact of silica nanoparticles upon introduction into the body is of great interest.

Once silica nanoparticles as intravascular carriers have entered the bloodstream by intravenous administration, endothelial cells lining the lumen of all blood vessels and the heart will have direct contact with them. The single layer of endothelial cells is not only just a biological barrier which mediating clearance of nanoparticles but also critical for the maintenance of vascular function and homeostasis [4,5]. Moreover, endothelium also serves as an important target for cell or gene therapies as they are involved in various pathophysiologic conditions such as atherosclerosis, myocardial infarction and restenosis [6]. Therefore, it is important to understand the interaction between nanoparticles and endothelial cells. However, in spite of their wide use as drug carriers or for gene therapy, there are only a few studies investigating adverse effects of silica nanoparticles on endothelial cells *in vitro*. Studies by *Dorota Napierska* demonstrated that smaller silica nanoparticles induced a higher cytotoxic response and affected exposed endothelial cells faster with cell death (by necrosis) [7]. Peters [8] also found that IL-8 release could be enhanced in endothelial cells by exposure to high dosage of silica nanoparticles. However, significant knowledge gaps currently exist concerning precise mechanisms of endothelial injury induced by silica nanoparticles.

Recently, oxidative stress has often been reported as toxic mechanism of silica nanoparticles-induced apoptosis and inflammation in various cell types including macrophages, embryonic kidney cells and epithelial cells [9–13], suggesting a potential role

* Corresponding author. Tel.: +86 21 63034903; fax: +86 21 63011643.
E-mail address: jiaosun59@yahoo.com (J. Sun).

0142-9612/$ – see front matter © 2010 Elsevier Ltd. All rights reserved.
doi:10.1016/j.biomaterials.2010.07.069

of reactive oxygen species (ROS) in changes of biological behavior in endothelial cells exposed to silica nanoparticles. However, the involvement of the oxidative stress responding signal transduction pathway in the toxicity of silica nanoparticles is poorly understood. ROS causing oxidative stress are known to activate members of the mitogen activated protein kinase (MAPK) family. The latter ones are important mediators of signal transduction, and play a key role in the regulation of many cellular processes, such as cell growth and proliferation, differentiation, and apoptosis [14]. The MAPK cascades are composed of three distinct signaling modules, the c-Jun N-terminal kinase (JNK) cascade, the p38MAPK cascade, and the extracellular signal-regulated kinase (ERK) cascade. In particular, JNK can induce apoptosis and is a key regulator of the transmission of pro-apoptotic signals [15]. The activation of MAPK pathway was also observed in endothelial cells exposed to nanosize copper (II) oxide or ambient ultrafine particles [16,17]. ROS could also induce p53 activation, followed cell-cycle arrest or apoptosis [18]. Our previous studies have reported that p53 activation was involved in hydroxyapatite nanoparticles-mediated apoptosis in macrophages [19]. Moreover, redox-sensitive transcription factor, such as nuclear factor kappaB (NF-κB) was recently investigated as target transcription factors of nanoparticles-mediated inflammation response [12,20]. Based on these evidences, it seems that the activation of JNK, p53 and NF-κB due to oxidative stress plays essential roles in silica nanoparticles-induced endothelial cells apoptosis and inflammation response.

In the present study, to investigate the basic mechanism underlying biological behavior of silica nanoparticles on endothelial cells, we conducted a battery of evaluations including oxidative stress, proinflammatory state, prothrombic properties and apoptosis response in human umbilical vein endothelial cells (HUVECs) after exposure to silica nanoparticles for 24 h. Moreover, we also measured the expression of p-JNK, p-p53, NF-κB and apoptosis-related protein to determine whether silica nanoparticles induce endothelial dysfunction through oxidative stress via JNK, p53 and NF-κB pathways.

2. Materials and methods

2.1. Silica nanoparticles synthesis, characterization and preparation

The silica nanoparticles were synthesized using a sol–gel process according to previously published procedures [21]. Briefly, one solution composed of ammonium hydroxide, deionized water and ethanol was slowly added to another solution containing tetraethylorthosilicate (TEOS) (Sigma, St. Louis, MO, USA) and ethanol, with stirring, and the final mixture was stirred overnight to allow the silica nanoparticles to coarsen. After two alcohol washes, silica nanoparticles were obtained by vacuum drying. The size and shape of the silica nanoparticles were examined under scanning electron microscope (SEM) (JEOL, Tokyo, Japan) and transmission electron microscope (TEM) (JEOL, Tokyo, Japan). Before inoculation into the *in vitro* systems, silica nanoparticles were sterilized by ethylene oxide. In this study, a series of silica nanoparticles concentrations ranging from 25 μg/mL (3×10^{12} NPs/mL) to 200 μg/mL (2.4×10^{13} NPs/mL) was chosen to test possible effects on HUVECs. Calculations for particle number concentrations (NPs/volume) were based on measured diameters from electron micrographs, mass concentrations (mass/volume) and densities of 2.0 g/cm^3 [22]. The final silica nanoparticles' dispersions were prepared freshly before use by serial dilution of the stock suspension (1 mg/mL) in ECM cell medium followed by intense vortexing. The concentrations we used were similar to the concentrations used in previously published *in vitro* or *in vivo* studies [7,11,13,23].

2.2. Cell preparation and culture

HUVECs were isolated and cultured using a modification of the method described by Jaffe et al. [24]. Briefly, the umbilical vein was rinsed thrice with phosphate-buffered saline (PBS) containing 100 U/mL penicillin/streptomycin (GIBCO, Scotland, UK), filled with 0.1% collagenase I (Sigma, St. Louis, MO, USA), and incubated for 15 min at 37 °C. Subsequently the cells were collected by perfusion with PBS and centrifugated at 1000 rpm for 10 min. After harvesting, the endothelial cells were placed in 75-cm^2 tissue culture flasks (Corning, US) and grown in endothelial cell medium (ECM) (Sciencell, San Diego, US). HUVECs between the third and sixth passage were used in our experiments. The phenotype of the endothelial cell was confirmed by performing immunofluorescence using monoclonal antibodies for the von Willebrand factor (Changdao Biotech, China).

To examine the effect of antioxidants on HUVECs after exposure to silica nanoparticles, HUVECs were treated with the mixture of 200 μg/mL nanoparticles with 20 mM *N*-acetyl cysteine (NAC) (Sigma, St. Louis, MO, USA) for 24 h, and then cells or supernatants were collected for a series of analysis according to experiment schedule.

2.3. Silica nanoparticles uptake using inductively coupled plasma mass spectrometry

The uptake of silica nanoparticles by HUVECs was detected using inductively coupled plasma mass spectrometry (ICP-MS) according to previous study [25]. HUVECs in 6-well plates were exposed to silica nanoparticles for 24 h, washed with PBS three times and trypsinized. After centrifugation at 1000 rpm, the cell pellet was washed with PBS once. The cells were resuspended in deionized water and counted and centrifuged again. After the cells were dried overnight, 50 wt% HF (100 μL) was added to allow dissolution of the silica nanoparticles with ultrasound. Then, 2 wt% HNO_3 (9.9 mL) in aqueous solution was added to allow dissolution of the cells with ultrasound. These clear acidic solutions were diluted to a volume of 50 mL and used for ICP-MS analysis. The mass of silica nanoparticles in the HUVECs was measured by detecting the silicon concentration with ICP-MS.

2.4. Cell viability assays

The cell viability was measured using MTS assay (Cell Titer 96_Aqueous non-radioactive cell proliferation assay) (Promega, Madison, WI). The HUVEC monolayer was approximately 70–80% confluent after 24 h of culture. Serial dilutions of silica nanoparticles were added and incubated for 24 h. A volume of 20 μL MTS was added to each well and incubated for 4 h at 37 °C within an atmosphere of 5% CO_2 and 100% humidity. The absorbance of formazan was measured at 490 nm using a microplate reader (Labsystems Dragon Wellscan MK3, Finland).

Lactate dehydrogenase (LDH) leakage, which is another measure of cytotoxicity on the basis of membrane integrity damage, was determined using a commercial LDH Kit (Jiancheng Bioengineering Co. Ltd, Nanjing, China) according to the manufacturer's protocols. After incubation with silica nanoparticles for 24 h, the supernatants of HUVECs were collected for LDH measurement. An aliquot of 100 μL cell medium was used for LDH activity analysis and the absorption was measured using a UV–visible spectrophotometer at 340 nm.

2.5. Assessment of necrosis and apoptosis

Apoptosis in endothelial cells was measured using the Annexin V-propidium iodide (PI) apoptosis detection kit (BD Biosciences, San Diego, USA). Briefly, HUVECs were exposed to silica nanoparticles for 24 h, washed with PBS three times and trypsinized. After centrifugation at 1000 rpm, the cell pellet was washed with PBS once and incubated with 5 μL Annexin V-FITC for 10 min, which was followed by staining with 5 μL PI. Then, the samples were diluted with 200 μL binding buffer and analyzed with a FACScan flow cytometer (Becton Dickinson, San Jose, CA), and at least 10^4 cells were counted for each sample. The cell population of interest was gated on the basis of the forward and side-scatter properties. Vertical and horizontal lines were designed based on autofluorescence of untreated control cells. The different labeling patterns in the Annexin V–PI analysis identified the different cell populations where FITC negative and PI negative were designated as viable cells; FITC positive and PI negative as early apoptotic cells; FITC positive and PI positive as late apoptotic cells or necrotic cells; and FITC negative and PI positive as necrotic cells. The data analysis was performed using Cell Quest software (Becton Dickinson, USA).

2.6. Intracellular ROS measurement

The production of intracellular reactive oxygen species (ROS) was measured by performing flow cytometry using the oxidation-sensitive probe, 2′,7′-dichlorofluorescein diacetate (DCFH-DA) (Applygen, Beijing, China). Briefly, 10 mM DCFH-DA stock solution (in methanol) was diluted 4000-fold in cell culture medium without serum or other additive to yield a 2.5 μM working solution. After the exposure of HUVECs to silica nanoparticles for 3 h and 24 h, respectively, the cells in 6-well plates were washed twice with PBS and incubated in 2 mL working solution of DCFH-DA at 37 °C in dark for 30 min. Then the cells were washed twice with cold PBS and resuspended in the PBS for analysis of intracellular ROS by a FACScan flow cytometer. DCFH fluorescence emission was collected with a 530-nm band-pass filter. The mean fluorescence intensity (MFI) of 10^4 cells was quantified using Cell Quest Software. The data were normalized to MFI values of the control cells.

2.7. Detection of changes in mitochondrial membrane potential (MMP)

Mitochondrial membrane permeability was determined using the Mitochondrial Permeability Detection Kit (Applygen, Beijing, China). The lipophilic dye JC-1 (5,5′, 6,6′-tetrachloro-1, 1′,3,3′-tetraethylbenzimidazolecarbocyanine iodide) was

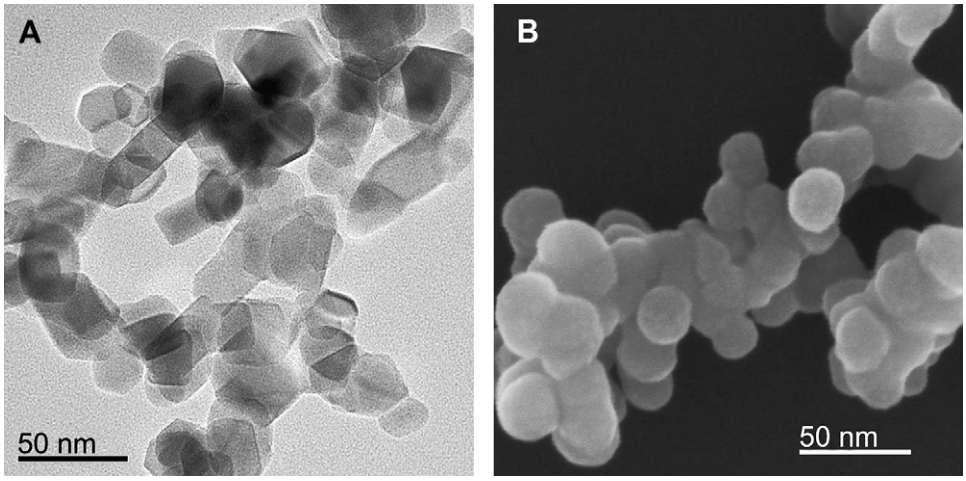

Fig. 1. TEM and SEM images for 20 nm silica nanoparticles. (A) TEM image; (B) SEM image.

used to measure the mitochondrial membrane potential ($\Delta\Psi$m). This dye reagent enters the mitochondria, aggregates, and fluoresces red. When the mitochondrial membrane potential collapses, the dye reagent can no longer accumulate within the mitochondria and fluoresces green. HUVECs were cultured with silica nanoparticles in 6-well plates for 24 h and then were rinsed with PBS twice, stained with 1 mL culture medium containing 5 μmol/L JC-1 for 30 min at 37 °C. Cells were rinsed with ice-cold PBS twice, resuspended in 200 μL ice-cooled PBS, and instantly assessed for red and green fluorescence with flow cytometry. A 488 nm filter was used for the excitation of JC-1. Emission filters of 535 and 595 nm were used to quantify the population of mitochondria with green (JC-1 monomers) and red (JC-1 aggregates) fluorescence, respectively. Frequency plots were prepared for FL1 (FITC) and FL2 (PE) to determine the percentage of the mitochondria stained green (loss membrane potential) and red (normal membrane potential).

2.8. Western blot analysis

Total cellular protein extracts were prepared as described in a previous study [26]. Briefly, HUVECs were stimulated with silica nanoparticles for 24 h, washed once with ice-cold PBS, and lysed in ice-cold lysis buffer [50 mM Tris–HCl, 150 mM NaCl, 1% NP-40, 0.1%sodium dodecyl sulfate (SDS), Applygen, Beijing, China] containing 1 mM phenylmethylsulphonyl fluoride (PMSF) (Sigma, St. Louis, MO, USA) and phosphatase inhibitor cocktail (Sigma, St. Louis, MO, USA) for 30 min. After centrifuging the lysates at 12,000 rpm, 4 °C for 10 min, the supernatants were collected and stored at −80 °C until use. The protein concentrations of these extracts were determined by performing the bicinchoninic acid (BCA) protein assay (Pierce, Rockford, USA). And then equal amounts of lysate proteins (40–80 μg) were loaded onto SDS-polyacrylamide gels (8–12% separation gels) and electrophoretically transferred to nitrocellulose (NC) membranes (Amersham Biosciences, US). After blocking with 5% nonfat milk in Tris-buffered saline (TBS) containing 0.05% Tween-20 (TBST) for 1 h at room temperature, the membrane was incubated with anti-p-ERK, ERK, p-JNK, JNK, p-c-Jun, c-Jun (1:1000, rabbit polyclonal antibodies, Bioworld Technology, USA), anti-Bcl-2 (1:2500, a mouse monoclonal antibody, clone: 118701, R&D Systems, Oxford, UK), anti-p-p53, NF-κB, Bax, caspase-3, β-actin (1:1000, rabbit polyclonal antibodies, CST, USA), and anti-Lamin B (1:1000, a goat polyclonal

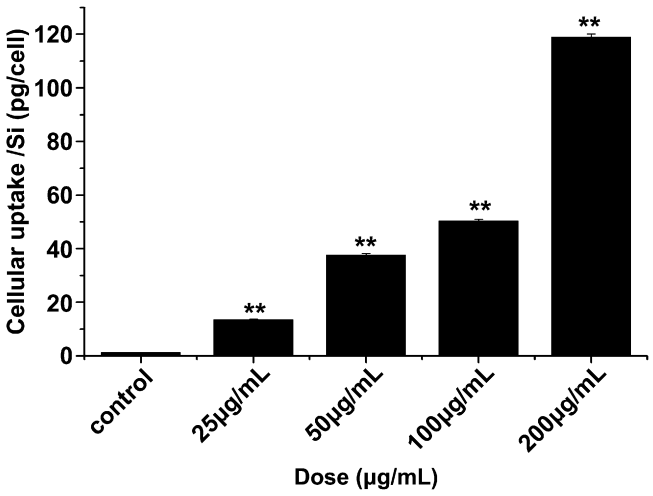

Fig. 2. Cell uptake of silica nanoparticles. HUVECs were exposed to increasing dose of silica nanoparticles for 24 h and the mass of silicon per cell was measured by ICP-MS. Data represents mean ± SD, $n = 3$. $^{**}p < 0.01$ vs. control.

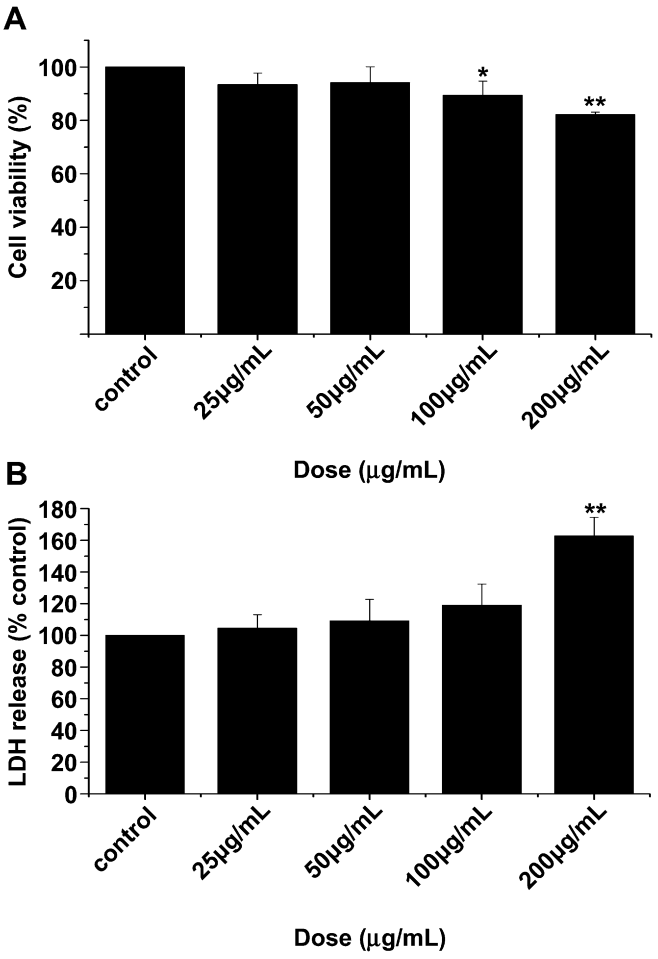

Fig. 3. Cell viability and LDH leakage of HUVECs exposed to increasing dose of silica nanoparticles for 24 h determined by the MTS and LDH assays. (A) The cell viability was measured with the MTS assay. (B) The LDH leakage in supernatants was measured by the LDH assay. Normal HUVECs without nanoparticles treatment served as control. Results are the mean ± SEM of three independent experiments each carried out in triplicate. $^{*}p < 0.05$; $^{**}p < 0.01$ vs. control.

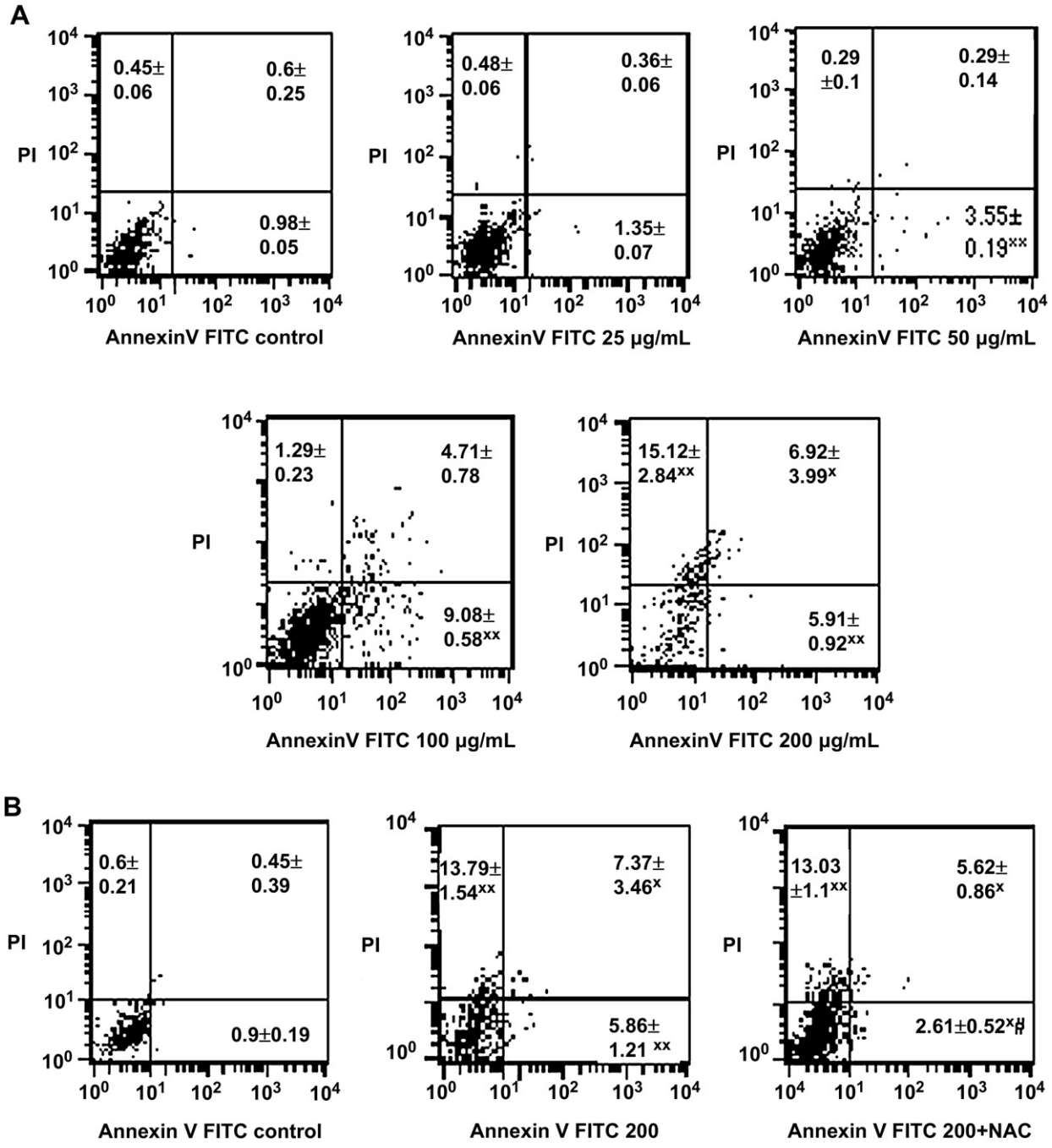

Fig. 4. Apoptosis induced by silica nanoparticles treatment in HUVECs. The graphs depict apoptotic and necrotic populations of cells double-stained with PI- and FITC-labeled Annexin V. HUVECs were treated with increasing concentrations of silica nanoparticles for 24 h and the distribution of viable, apoptotic and necrotic cells was analyzed (4A). HUVECs were treated with the mixture of 200 μg/mL silica nanoparticles and NAC for 24 h and assayed for apoptosis (4B). Normal HUVECs without nanoparticles treatment served as control. Numbers in quadrant indicate percentage of cells and data represents mean ± SD, $n = 3$. $^{*}p < 0.05$, $^{**}p < 0.01$ vs. control. $\#p < 0.05$ vs. silica nanoparticles treated group (200 μg/mL).

antibody, Santa Cruz Biotechnology, CA) overnight at 4 °C, washed with TBST, and incubated with a horseradish peroxidase-conjugated anti-rabbit IgG/anti-mouse IgG/anti-goat IgG secondary antibody for 1 h at 37 °C. The antibody-bound proteins were detected using the ECL chemiluminescence reagent (Millipore, USA).

2.9. Immunofluorescent staining of HUVECs for flow cytometry

The levels of HUVECs surface CAMs expression were assessed by flow cytometry. After exposure to silica nanoparticles for 24 h, HUVECs were released from the wells after PBS washing and then labeled with saturating levels of fluorescently labeled monoclonal antibodies specific for cell surface activation markers at root temperature (RT) for 45 min in the darkness. The following mouse anti-human monoclonal antibodies were used: ICAM-1 (CD54-PE, eBioscience, San Diego, USA), VCAM-1 (CD106-FITC, BD Biosciences, San Diego, USA), E-selectin (CD62E-APC, BD Biosciences, San Diego, USA). All samples were analyzed by BD flow cytometer. The data were analyzed using Cell Quest software.

2.10. Cytokine measurement

For the assay of cytokines [Interleukin (IL)-6, IL-8, monocyte chemotactic protein-1 (MCP-1), TNF-α and tissue factor (TF)], the medium from HUVECs exposed to silica nanoparticles was collected after 24 h, immediately centrifuged free of cells, and then frozen at −80 °C until analyzed. The amount of TNF-α, IL-6, MCP-1, IL-8 and TF was quantified by an Immunoassay Kit (R&D Systems, Oxford, UK) according to manufacturer's instructions.

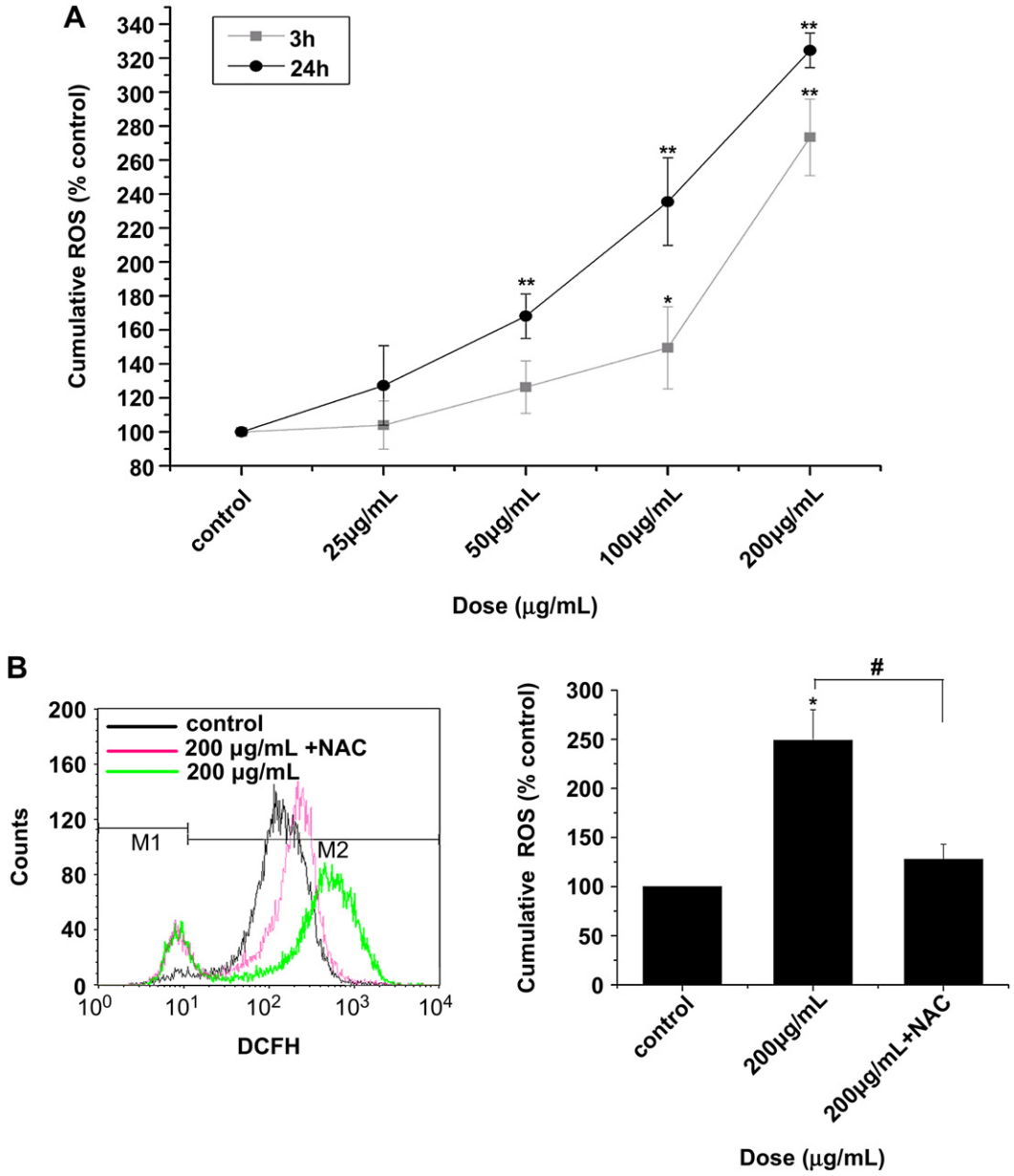

Fig. 5. Effect of silica nanoparticles on ROS production in HUVECs. (A) ROS generation in HUVECs exposed to increasing concentrations of silica nanoparticles for 3 h and 24 h. (B) NAC inhibited the increased ROS in HUVECs exposed to 200 μg/mL of silica nanoparticles. ROS generation was depicted by histogram of flow cytometry analysis. Bar graph shows the inhibited effects of NAC on silica nanoparticle-induced ROS production. Normal HUVECs without nanoparticles treatment served as control. Data represents mean ± SD, $n = 3$. $^{*}p < 0.05$, $^{**}p < 0.01$ vs. control. $\#p < 0.05$ significant difference as compared groups.

2.11. Electrophoretic mobility shift assay (EMSA)

The EMSA is classically used to detect the activity of transcription factors and other sequence specific DNA-binding proteins, the principle is that DNA with protein bound, has less mobility through a polyacrylamide gel matrix than the corresponding free unbound DNA. In this study, the NF-κB activation of HUVECs was assessed by EMSA. In brief, HUVECs were stimulated by silica nanoparticles for 24 h. Nuclear extracts of HUVECs were prepared as described by Nuclear and Cytoplasmic Extraction Reagents (Pierce, Rockford, USA). Protein concentrations were quantified by BCA protein assay. An amount of 10 μg of nuclear protein was incubated in binding buffer containing 50 ng/μL Poly (dI•dC), 2.5% Glycerol, 0.05% NP-40, 5 mM $MgCl_2$ and 20 fmol Biotin end-Labeled oligonucleotides for 20 min at RT. The labeled oligonucleotides had the following sequences: 5′-AGT TGA GGG GAC TTT CCC AGG C-3′; 5′-GCC TGG GAA AGT CCC CTC AAC T-3′. The specificity of binding was examined by competition with unlabeled oligonucleotide. For competition experiments, a 1000-fold excess of cold oligonucleotide was used. For the supershift assay, nuclear protein of HUVECs exposed to 200 μg/mL silica nanoparticles was incubated with anti-p65 antibody (Santa Cruz Biotechnology, Santa Cruz, CA) for 30 min at RT before the addition of oligonucleotides. Protein–DNA complexes were separated from free DNA probe by electrophoresis through 4% native polyacrylamide gels. Gels were dried and then protein–DNA complexes were visualized by the ECL chemiluminescence systems.

2.12. Statistical analysis

Data are expressed as mean ± SD or mean ± SEM. The statistical comparisons of means were performed using one-way analysis of variance (ANOVA) using the software SAS 6.12. The differences were considered to be significant when the p value was less than 0.05.

3. Results

3.1. Characterization of silica nanoparticles

Prior to the study of impact of silica nanoparticles on HUVECs, characterization of synthesized silica nanoparticles was performed

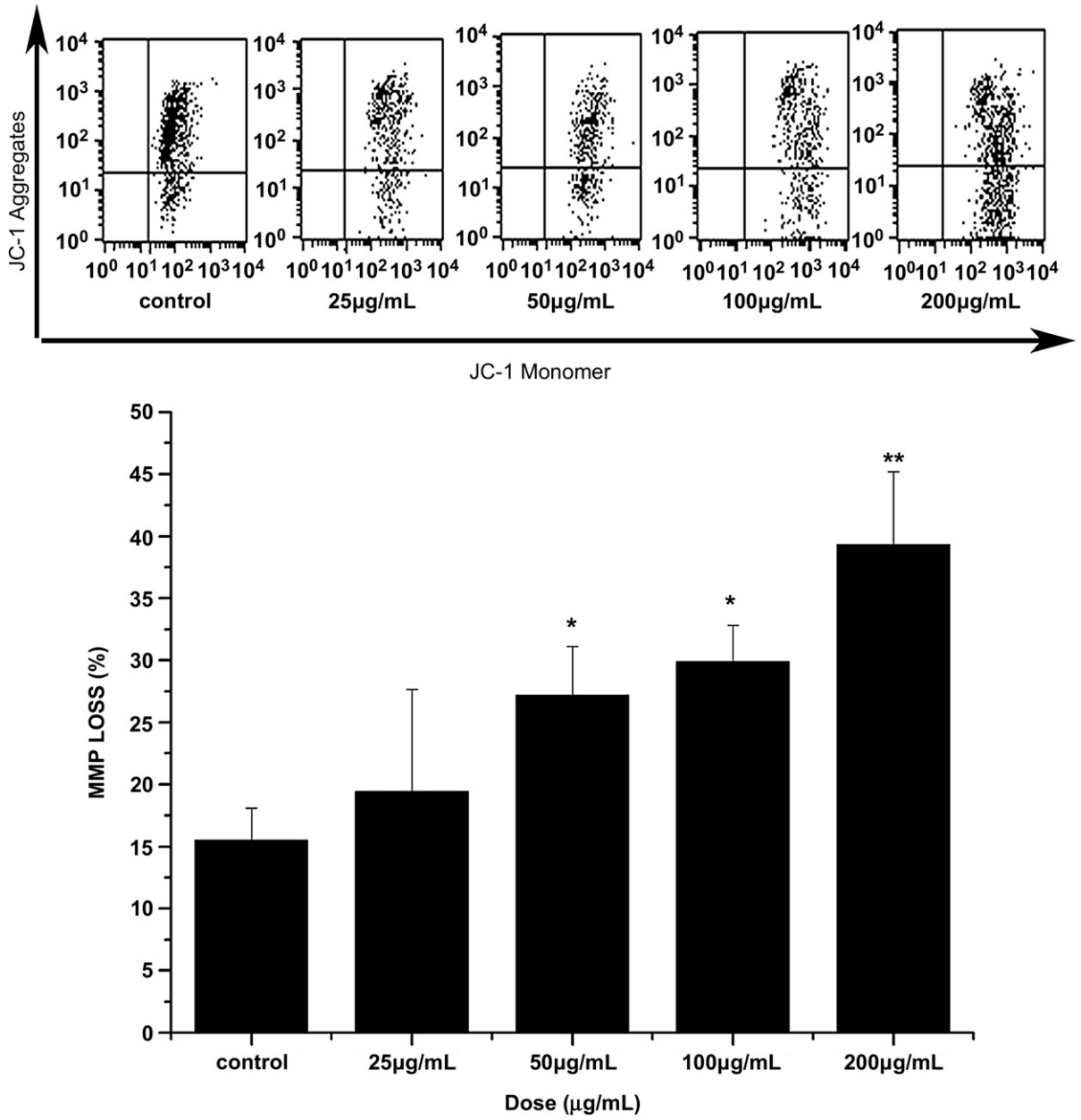

Fig. 6. Effect of silica nanoparticles on MMP of HUVECs. HUVECs were treated with different concentrations of silica nanoparticles for 24 h and then stained for the JC-1 followed by flow cytometry analysis. Dot-plot of flow cytometry analysis shows the distribution of JC-1 aggregates and JC-1 monomer in the mitochondrial membrane and cytoplasm, respectively. Bar graph shows the percentage of JC-1 monomer positive cells. Normal HUVECs without nanoparticles treatment served as control. Data represents mean ± SD, $n = 3$. $^{*}p < 0.05$, $^{**}p < 0.01$ vs. control.

using TEM and SEM methods. As shown in Fig. 1, the TEM and SEM images of silica nanoparticles from the test medium confirmed that the nanoparticles types were near-spherical and the sizes approximately matched the sizes measured after synthesis (20 nm).

3.2. Uptake of silica nanoparticles by HUVECs

To understand the interactions of silica nanoparticles with HUVECs, the uptake of silica nanoparticles by HUVECs was first measured using ICP-MS. As shown in Fig. 2, ICP-MS measurements revealed that the amount of silicon uptake correlated directly with the concentration of silica nanoparticles. This result indicated a clear dose-dependent increase in the uptake of the silica nanoparticles by HUVECs.

3.3. Cytotoxic effects of silica nanoparticles on HUVECs

To assess the biological effect of silica nanoparticles on endothelial cells, cell viability was determined after exposing HUVECs to various concentrations (25, 50, 100, and 200 μg/mL) of silica nanoparticles for 24 h. As shown in Fig. 3A, HUVECs exposure to 25 and 50 μg/mL of silica nanoparticles did not show any significant change in cell viability, while at the highest concentrations (200 μg/mL), cell viability decreased to 82.23%, significantly lower than control. To reveal the impact of nanoparticles on cell-membrane integrity, LDH leakage was measured. As indicated in Fig. 3B, no significant difference of LDH release was observed when incubated with 25, 50 and 100 μg/mL of silica nanoparticles for 24 h compared to control ($p > 0.05$), while at the highest concentration

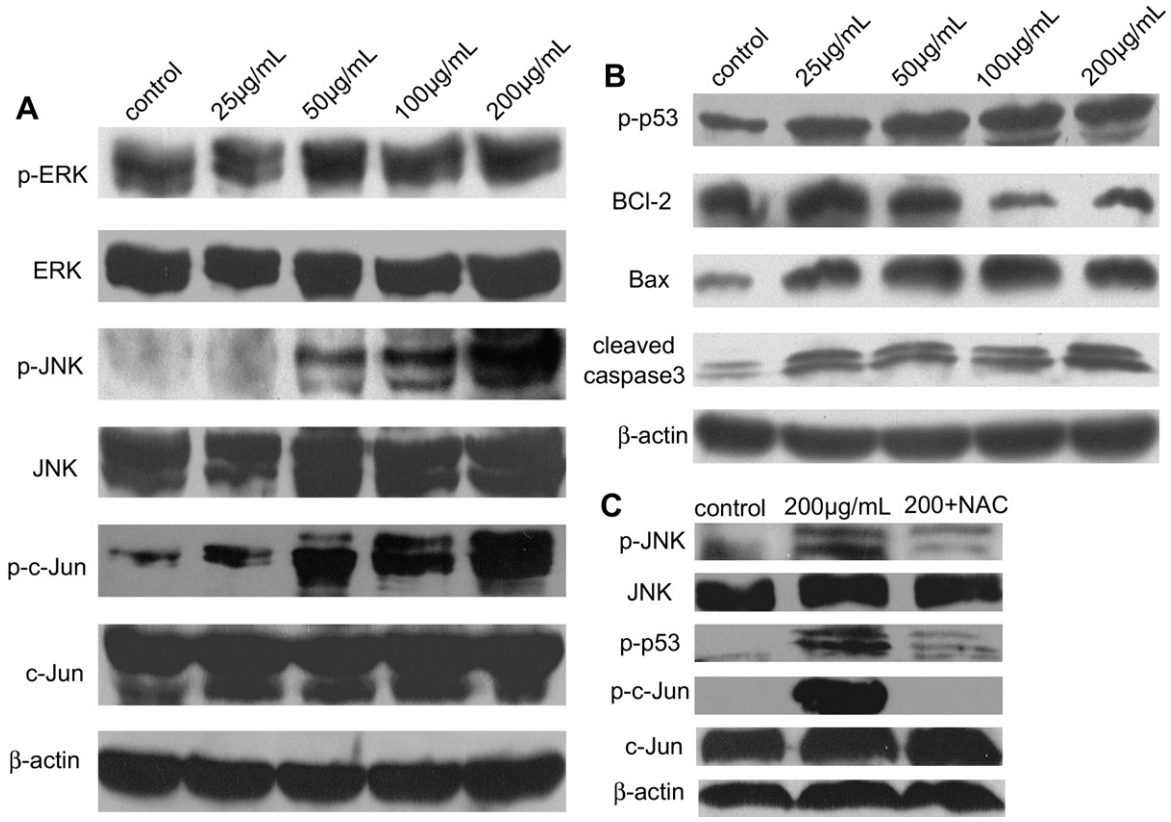

Fig. 7. Effects of silica nanoparticles on the MAPK and apoptotic signaling pathways. HUVECs were exposed to different concentrations of silica nanoparticles for 24 h. Aliquots of cell lysates were separated by SDS-PAGE and analyzed for protein expression by Western blotting as described in Section 2. β-actin was used as an internal control to monitor for equal loading. (A) Effect of silica nanoparticles on the expression of p-ERK/ERK, p-JNK/JNK, p-c-Jun/c-Jun. (B) Effect of silica nanoparticles on the expression of p-p53, Bax/Bcl-2, cleaved caspase-3. (C) Effect of NAC on silica nanoparticles-induced p-JNK, p-c-Jun, p-p53 expression. The results shown are representative of three independent experiments.

(200 μg/mL), the LDH release was significantly elevated (~1.6 fold greater than the negative control). This result showed that cell-membrane damage could be induced when HUVECs had been exposed to 200 μg/mL of silica nanoparticles.

3.4. Apoptosis and necrosis in HUVECs triggered by silica nanoparticles

To further investigate the extent of damage by silica nanoparticles, apoptosis and necrosis in HUVECs were assessed by flow cytometry. After 24 h of exposure, at the doses up to 50 μg/mL, the apoptotic rate was increased in HUVECs and peaked at 100 μg/mL; then at 200 μg/mL it decreased to considerably lower levels, which, however, were still significantly higher than those of the control. In contrast, the dose of only 200 μg/mL of silica nanoparticles was capable of causing necrosis (Fig. 4A). Interestingly, ROS scavenger (NAC) only decreased apoptosis, but not necrosis (Fig. 4B). The flow cytometry results were in accordance with the LDH result.

3.5. Oxidative stress induced by silica nanoparticles in HUVECs

To investigate the induction of oxidative stress in HUVECs by silica nanoparticles, ROS generation was monitored through increases in fluorescence intensity of dichlorofluorescein (DCF). As shown in Fig. 5A, exposing HUVECs to 100 μg/mL of silica nanoparticles significantly increased ROS generation at as early as 3 h ($p < 0.05$). With time increasing, HUVECs exposed to as low as 50 μg/mL of silica nanoparticles for 24 h also showed a significant increase in ROS generation ($p < 0.01$). This result indicated that DCF fluorescence increased progressively in a time- and dose-dependent manner. Furthermore, the increase in the DCF fluorescence with the exposure to nanoparticles was abolished by coincubation of silica nanoparticles with NAC for 24 h (Fig. 5B).

3.6. Mitochondrial damage induced by silica nanoparticles

One of the crucial events in apoptotic signaling is the alteration of mitochondrial membrane integrity. Therefore, the effect of silica nanoparticles on the MMP of HUVECs was evaluated using JC-1 mitochondrial membrane potential detection kit. Treatment of HUVECs with 50, 100 and 200 μg/mL silica nanoparticles significantly increased green fluorescent JC-1 aggregates to 27.17% ± 3.94, 2 9.89% ± 2.94 and 39.32% ± 5.9 compared with the control values of 15.48% ± 2.63 ($p < 0.05$) (Fig. 6). The results demonstrated that mitochondrial depolarization was induced by the silica nanoparticles in a dose-dependent manner.

3.7. The activation of JNK and p53 dependent pathways by silica nanoparticles

To better understand the apoptotic signaling pathway, we examined the expression of apoptotic regulators in HUVECs by western blot analysis. As shown in Fig. 7A, JNK and c-Jun phosphorylation were increased in a dose–response manner in HUVECs exposed to 50, 100, and 200 μg/mL silica nanoparticles for 24 h, whereas the expression of total JNK and c-Jun was not changed. In contrast to the changes observed in p-JNK and p-c-Jun expression, p-ERK and total ERK were not upregulated in HUVECs exposed to any doses from 25 μg/mL to 200 μg/mL. Interestingly, pro-apoptotic protein such as p-p53, Bax and caspase-3 were significantly increased after incubation with as

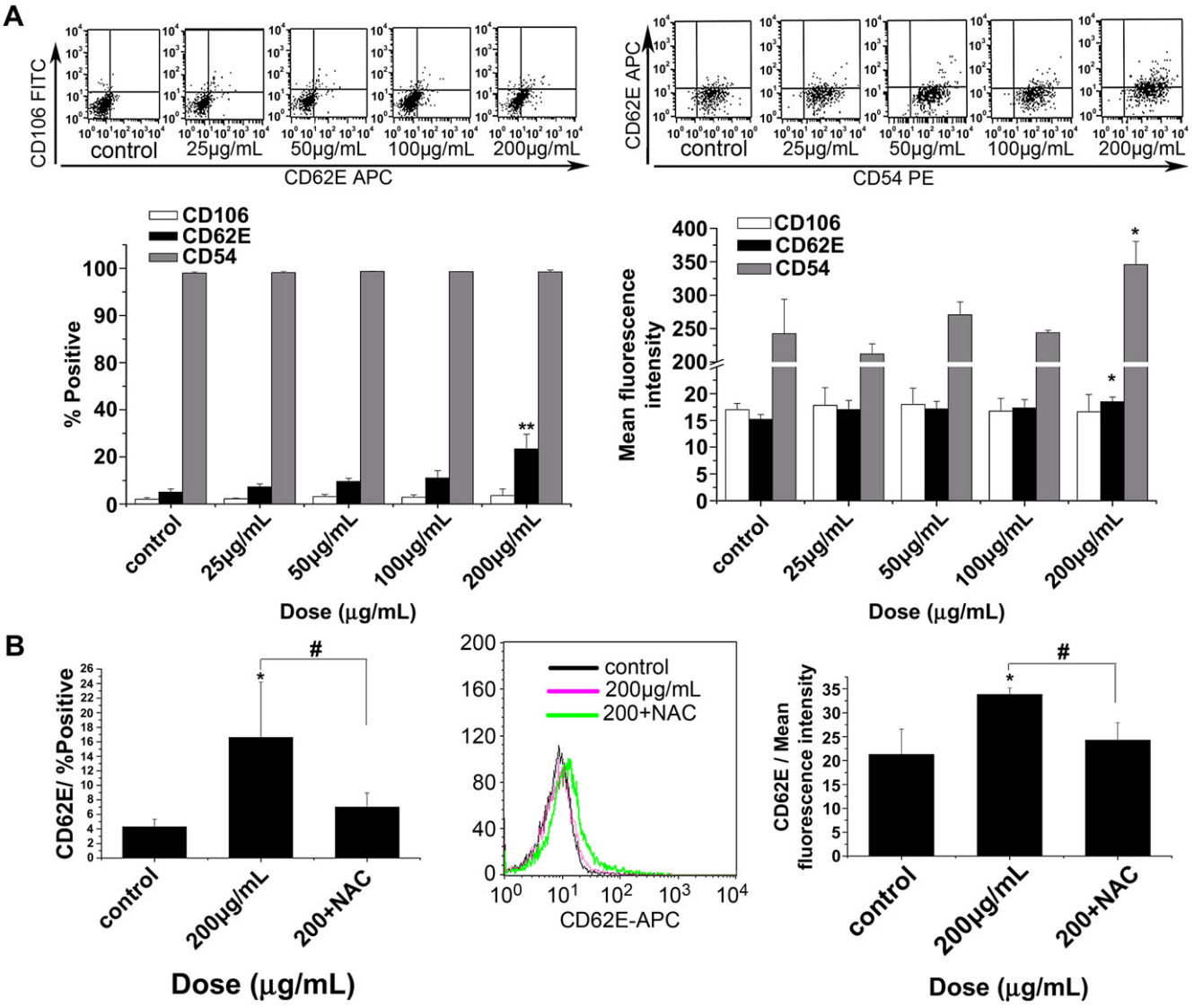

Fig. 8. CAMs expression on HUVEC exposed to silica nanoparticles for 24 h. (A) Dot-plot of flow cytometry analysis showing the expressions of CD54, CD106, and CD62E on HUVECs exposed to different concentrations of silica nanoparticles for 24 h. Bar graph shows the mean fluorescence intensity and the percentage of CD54, CD106, and CD62E positive cells. (B) NAC inhibited CD62E expression in HUVECs exposed to 200 μg/mL of silica nanoparticles. The expression of CD62E was depicted by histogram of flow cytometry analysis. Bar graph shows the inhibited effects of NAC on silica nanoparticle-induced CD62E expression. Normal HUVECs without nanoparticles treatment served as control. Data represent means ± SEM; $n = 3$. $^{*}p < 0.05$, $^{**}p < 0.01$ vs. control. #$p < 0.05$ significant difference as compared groups.

low as 25 μg/mL of silica nanoparticles, while anti-apoptotic protein Bcl-2 was dramatically suppressed after exposure 100 μg/mL and 200 μg/mL of silica nanoparticles (Fig. 7B). Western blot analysis showed that JNK, c-Jun and p53 activation were effectively inhibited by the addition of ROS scavenger (Fig. 7C).

3.8. Increase in endothelial adhesion molecule expression by silica nanoparticles

Having established that silica nanoparticles could induce HUVECs apoptosis and necrosis, we questioned whether silica nanoparticles could also mediate endothelial activation. Thus, the expression of CD54, CD106 and CD62E on HUVECs exposed to different concentrations of silica nanoparticles was proved by the increased mean fluorescence intensity and the percentage of positive cells using flow cytometry. As depicted in Fig. 8A, the expression of CD54 and CD62E on HUVECs incubated with the concentrations (25, 50 and 100 μg/mL) was not greatly altered, but only the concentration of 200 μg/mL showed significant increase ($p < 0.01$). In addition, there were not any significant changes in expression of CD106 after exposure to silica nanoparticles at all concentrations tested. Co-treatment of silica nanoparticles with NAC significantly downregulates the expression of CD62E (Fig. 8B).

3.9. Induction of proinflammatory and procoagulant factor production by HUVECs mediated by silica nanoparticles

To further evaluate inflammatory response and endothelial activation induced by nanoparticles, we measured proinflammatory and procoagulant factor production by HUVECs after exposure to silica nanoparticles for 24 h. TNF-α, IL-6, IL-8 and MCP-1 were chosen as the indicators of inflammatory response, and TF was selected as a procoagulant marker. As shown in Fig. 9A, in comparison to control, only high concentrations (100, 200 μg/mL) of silica nanoparticles generated a significant increase in proinflammatory cytokine secretion including IL-6 (∼22 fold), IL-8

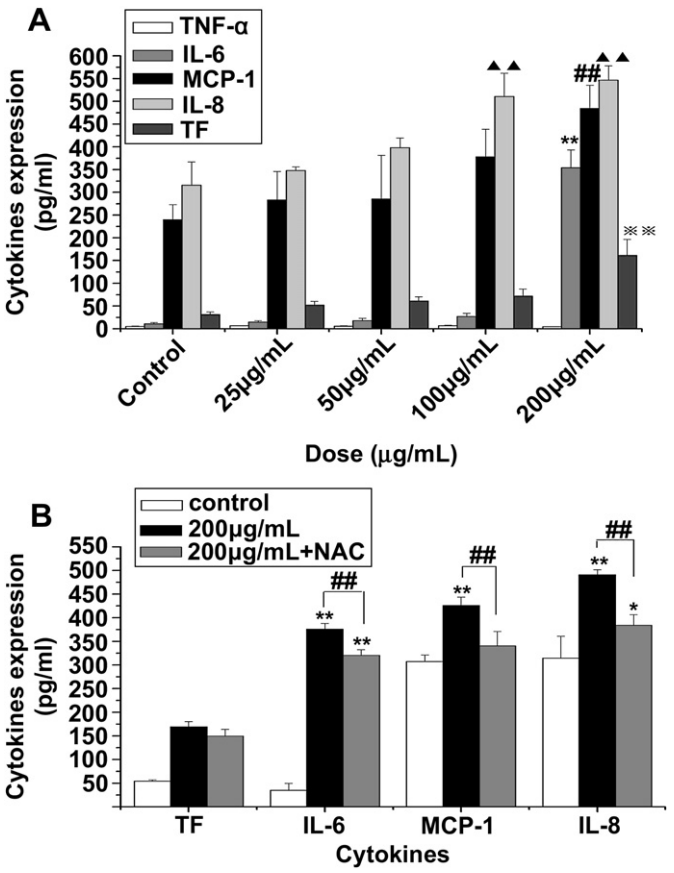

Fig. 9. Effect of silica nanoparticles on cytokine release from HUVECs. (A) TNF-α, IL-6, MCP-1, IL-8 and TF release from HUVECs exposed to different dose of silica nanoparticles for 24 h. Normal HUVECs without nanoparticles treatment served as control. Data represent means ± SD, $n = 3$. ▲▲, ##, **, ※※ $p < 0.01$ vs. control. (B) Effect of NAC on TF, IL-6, MCP-1 and IL-8 release from HUVECs exposed to 200 μg/mL of silica nanoparticles. Data represents mean ± SD, $n = 3$. *$p < 0.05$, **$p < 0.01$ vs. control, ##$p < 0.01$ significant difference as compared groups.

(~1.6fold) and MCP-1 (~1.7fold) ($p < 0.01$). Meanwhile, TF release also significantly increased (~5 fold) when HUVECs were exposed to 200 μg/mL silica nanoparticles. By contrast, TNF-α production was not affected by any doses of silica nanoparticles. Moreover, coincubation of silica nanoparticles with NAC slightly attenuated the release of IL-6, IL-8 and MCP-1 (Fig. 9B).

3.10. Activation of NF-κB by silica nanoparticles in HUVECs

To clarify the possible mechanism of endothelial cells activation induced by silica nanoparticles, the activation of NF-κB was investigated by exposing HUVECs to silica nanoparticles for 24 h and performing western blot analysis and EMSA. Fig. 10A shows that 200 μg/mL silica nanoparticles induced the nuclear localization of the NF-κB p65 subunit. Consistent with this observation, results in Fig. 10B also clearly show the activation of NF-κB at the highest concentrations (200 μg/mL) of silica nanoparticles. The result also showed that silica nanoparticles-induced NF-κB activation was inhibited by NAC (Fig. 10C).

4. Discussion

Silica nanoparticles represent a promising class of nanomaterials that offers several attractive features for diagnostics and targeting cells in drug delivery [27]. A key administration route of silica nanoparticles is intravenous injection, thus endothelial cells will be the primary cells exposed to these nanoparticles. To date, a complete understanding of how silica nanoparticles interact with endothelial cells, especially at the molecular level, is still unclear. Our findings demonstrated that direct exposure of HUVECs to silica nanoparticles-induced intracellular ROS generation leading to the activation of JNK/p53 and NF-κB pathways, and subsequently to the dysfunction of endothelial cells.

In this study, we found silica nanoparticles at concentrations ranging 25–200 μg/mL could be taken up by HUVECs in a dose-dependent manner (Fig. 2). This result indicated that all particle concentrations we used in the cell culture medium could lead to a related dose delivered to the cells. Subsequently, to further assess the biological effect of different concentrations of silica nanoparticles on endothelial cells, cell viability was first determined. Our MTS results showed exposure to high concentrations (100–200 μg/mL) of silica nanoparticles caused an increase of cytotoxicity in HUVECs (Fig. 3A). The LDH release was also increased by silica nanoparticles only at the highest concentration (Fig. 3B), indicating that exposure to high concentrations of silica nanoparticles can affect cell-membrane integrity and lead to cell death. To better confirm and analyze this observation, apoptosis/necrosis was also measured in the present study. After exposure to silica nanoparticles for 24 h, apoptosis was predominant at low concentrations (50–100 μg/mL). Consistent with LDH results, only at the highest concentration of 200 μg/mL, a significant increase in the percentage of PI positive cells was noted, indicating necrosis (Fig. 4A). Induction of apoptosis or necrosis by silica nanoparticles in a variety cell types has been observed, and oxidative stress as silica nanoparticles-induced toxicity mechanism has been reported [11–13]. Consistent with previous reports, our data showed that intracellular ROS generation of HUVECs by silica nanoparticles was gradually increased in a time- and dose-dependent manner (Fig. 5A), suggesting that oxidative stress occurred not at once, but continuously during cell culture. More recently, it has become clear that the endothelium generation of ROS is implicated in vascular tone, cell growth and proliferation, apoptosis, and inflammatory responses [5,28,29]. However, our data unexpectedly demonstrated that ROS scavenger only effectively inhibited silica nanoparticles-mediated apoptosis but had no effect on necrosis, indicating that ROS played a central role in silica nanoparticles-mediated apoptosis, whereas necrosis by silica nanoparticles was not completely dependent on oxidative stress (Fig. 4B). Disturbance of membrane integrity has been recently suggested as possibly one of the mechanisms for cytotoxic action in nanoparticles [30]. Previous studies have shown that polycationic organic nanoparticles cause holes in plasma membranes and the formation of such holes was linked to cellular uptake of particles [31]. TEM results by other study also showed apparent discontinuities in the cell membrane in endothelial cells treated with ZnO nanoparticles [32]. A higher cellular uptake for silica nanoparticles by HUVECs was also observed at high concentrations in our study (Fig. 2). Thus, it is likely that high concentrations of silica nanoparticles could damage plasma membranes of endothelial cells and cause necrosis. Moreover, previous studies reported that endothelial cells predominantly showed necrosis but not apoptosis after exposure to silica nanoparticles at the LD_{50} concentrations for 6 h [7]. However, our data demonstrated that exposure to any dose silica nanoparticles from 50 to 200 μg/mL could also induce apoptosis in HUVECs. Endothelial cells apoptosis was thought to be involved in atherosclerosis and thrombosis [33]. Therefore, it is necessary to further investigate the cell signaling pathway of nanoparticles-mediated apoptosis.

Mechanisms involved in the induction of apoptosis through oxidative stress by silica nanoparticles are not yet to be determined. Oxidative stress is associated with protein and lipid oxidation, ultimately leading to a profound alteration in

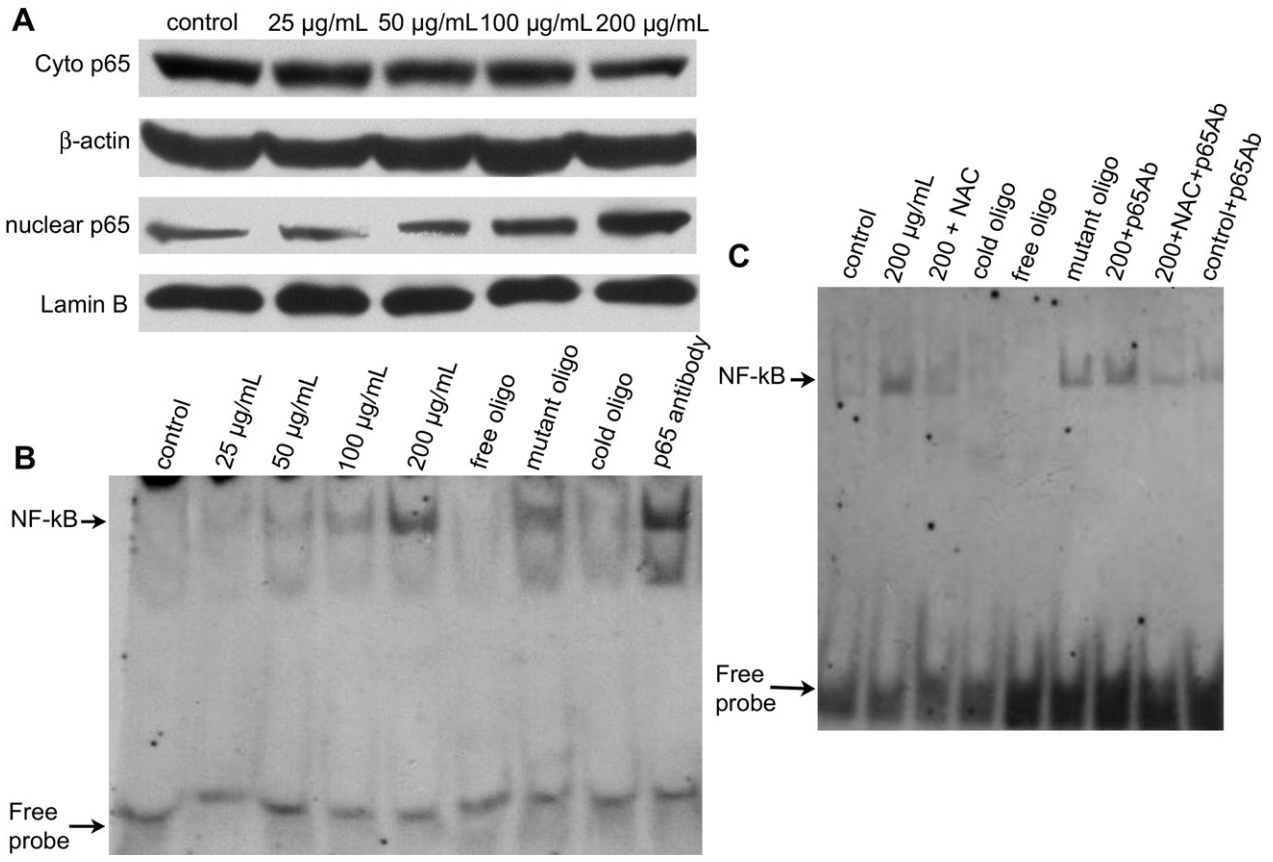

Fig. 10. Effect of silica nanoparticles on NF-κB activation. HUVECs were treated with different concentrations of silica nanoparticles for 24 h. Cells from these treatments were washed in chilled buffer to prepare cytoplasmic and nuclear extracts. (A) Western blotting was used to examine the effects of silica nanoparticles on NF-κB activation. (B) NF-κB DNA-binding activity was assayed by electrophoretic mobility shift assay (EMSA) as described in Section 2. (C) EMSA was used to detect the inhibited effect of NAC on silica nanoparticles-induced NF-κB activation. The detection of band supershift and specificity of NF-κB activation were measured with p65 antibodies, unlabeled oligo-, mutated NF-κB oligonucleotides.

mitochondrial function [34]. Any change in the mitochondrial membrane permeability is known to be an early event in apoptosis. Our study showed a clear dose–response in mitochondrial depolarization following exposure to silica nanoparticles (Fig. 6), which suggests that mitochondria are involved in silica nanoparticle-induced apoptosis. Mitochondria-dependent apoptosis has been previously reported in response to other nanoparticles, i.e. nanosilver and hydroxyapatite nanoparticles [35,36]. It is known that ROS activates multiple signaling pathways, including MAPK and p53 signal transduction cascades [37,38]. P53, Bax and Bcl-2 are also generally thought to be involved in mitochondria-dependent apoptosis. In this study, we found that p-JNK, p-c-Jun, p-p53, Bax, cleaved caspase-3 were significantly increased in HUVECs after exposure to silica nanoparticles, while Bcl-2 was dramatically suppressed (Fig. 7A, B). In addition, it is worthwhile to note that p-p53, Bax and activated caspase-3 were upregulated by silica nanoparticles at concentrations as low as 25 μg/mL, suggesting that non-toxic dose of silica nanoparticles could also cause endothelial cells injury at molecular level. ROS scavenger could markedly inhibit JNK, c-Jun and p53 activity, indicating that ROS may be upstream effectors of JNK and p53 (Fig. 7C). Consistent with our results, Yi-Hong Hsin also demonstrated that nanosilver-induced apoptosis was mediated by ROS via JNK and p53 activation [35]. ROS, JNK and p53 activation play an important role in regulating apoptosis. ROS could activate JNK, which in turn phosphorylates its substrates such as c-Jun and p53 [39]. In addition, ROS could also directly activate p53, most probably by the induction of DNA damage [38]. P53 is known to induce expression of Bax, which is a pro-apoptotic Bcl-2 family member and downregulate anti-apoptotic protein Bcl-2 level, resulting in increased mitochondrial membrane permeability, cytochrome *c* release, caspase-3 activation, and apoptosis [18]. Based on evidence from our study, the following silica nanoparticles-mediated signaling pathway for apoptosis-related events is proposed: Exposure to silica nanoparticles → ROS production → (JNK/c-Jun phosphorylation) → P53 activation → Bax upregulation/Bcl-2 downregulation → Loss of $\Delta\Psi$m → caspase-3 activation → apoptosis.

In the present study, in addition to their capacity to induce apoptosis, at the highest concentrations of 200 μg/mL, silica nanoparticles were also capable of inducing CD54 and CD62E expression and the generation of cytokines such as IL-8, IL-6, MCP-1,TF in HUVECs (Figs. 8A and 9A). Our results are almost consistent with those from these studies showing that higher dose exposure to nanomaterials including titanium dioxide, zinc oxide, alumina nanoparticles led to proinflammatory and procoagulant responses in endothelial cells [32,40,41]. The proinflammatory, procoagulant state of activated endothelial cells is implicated in many pathologic conditions of cardiovascular disease, including thrombus, atherosclerosis, diabetic vasculopathy, hypertension, coronary artery disease, chronic heart failure [5]. In addition, the endothelium is the primary barrier to nanoparticle delivery. When the integrity of the endothelial barrier is perturbed by inflammatory processes, nanoparticles escape from the vasculature and cause unexpected effects in nanomedicine therapy [42].

It is an accepted view point that ROS are involved in many of the processes underlying endothelial activation (e.g., the upregulation

of adhesion molecules and chemokines, increased expression of tissue factor). Many of the key signal transduction molecules involved in endothelial activation, such as various MAPKs and the transcription factors NF-κB, are known to be redox sensitive [5]. NF-κB exists in the cytoplasm in its inactive form as the protein heterodimer p50/p65 associated with an inhibitor protein IκB. The activation of NF-κB is dependent on IκB kinases which phosphorylate IκB leading to its degradation with subsequent liberation and translocation of NF-κB to the nucleus [43]. NF-κB activation was previously reported in keratinocytes exposed to single-walled carbon nanotube [20]. Our results demonstrated that HUVECs treated with silica nanoparticles decreased their expression of NF-κB in cytoplasm, meanwhile increased the level of NF-κB in nucleus, indicating NF-κB activation through translocation of NF-κB to the nucleus (Fig. 10A). The result of EMSA assay further showed that the silica nanoparticles stimulation increased NF-κB activity in HUVECs (Fig. 10B). In addition, ROS scavenger effectively inhibited NF-κB activity and significantly downregulated the expression of CD62E and MCP-1 generation (Fig. 8B, Fig. 9B, Fig. 10C), whereas TF production was not changed (Fig. 9B). Thus, it is likely that ROS take part in endothelial cells activation, but ROS generation is not the only pathway to consider for the induction of inflammation response and prothrombic effects to nanoparticles.

Endothelial dysfunction is characterized by a shift of the actions of the endothelium toward reduced vasodilation, a proinflammatory state, and prothrombic properties and apoptosis response [44]. Our results showed that exposure to silica nanoparticles could induce ROS production following endothelial cells dysfunction, but the mechanism of ROS generation in HUVECs induced by silica nanoparticles remains elusive. Our study demonstrated that apoptosis was induced by JNK/p53 pathway and proinflammatory response was mediated by NF-κB pathway, but the cross-talk between these two pathways is not clear. Moreover, we also found silica nanoparticles at higher concentrations could cause HUVECs necrosis, thus further studies are needed to investigate the mechanism of higher concentration of silica nanoparticles on cell necrosis. Finally, we evaluated the biological effects of silica nanoparticles on endothelial cells under static conditions. Endothelial cells *in vivo* are constantly exposed to blood flow, and there is evidence that shear stress regulates endothelial inflammation or apoptosis. Therefore, future investigation under simulated flow is needed to provide a more precise mechanism of endothelial cell dysfunction induced by nanoparticles.

5. Conclusion

In summary, data from the current study show that exposure to silica nanoparticles causes endothelial cells ROS generation, which induces apoptosis via JNK/p53 dependent mitochondrial pathways. Exposure to silica nanoparticles at high concentrations also causes activation of NF-κB due to oxidative stress in endothelial cells, which results in the upregulation of CD54, CD62E, TF, IL-6, IL-8 and MCP-1. Moreover, our overall findings suggest that exposure to silica nanoparticles is possibly a significant risk for the development of cardiovascular diseases such as atherosclerosis and thrombus.

Acknowledgment

This work was supported by grants from Natural Science Foundation of China (no. 30670556, no. 30470479), Shanghai Sci-Tech Committee Foundation (0752nm026) and Shanghai Leading Academic Discipline Project (no. S30206).

Appendix

Figures with essential color discrimination. Figs. 5 and 8 in this article have parts that are difficult to interpret in black and white. The full color images can be found in the on-line version, at doi:10.1016/j.biomaterials.2010.07.069.

References

[1] Tan W, Wang K, He X, Zhao XJ, Drake T, Wang L, et al. Bionanotechnology based on silica nanoparticles. Med Res Rev 2004;24:621–38.
[2] Luo D, Han E, Belcheva N, Saltzman WM. A self-assembled, modular DNA delivery system mediated by silica nanoparticles. J Control Release 2004;95:333–41.
[3] Lu J, Liong M, Zink JI, Tamanoi F. Mesoporous silica nanoparticles as a delivery system for hydrophobic anticancer drugs. Small 2007;3:1341–6.
[4] Albini A, Mussi V, Parodi A, Ventura A, Principi E, Tegami S, et al. Interactions of single-wall carbon nanotubes with endothelial cells. Nanomedicine 2010;6:277–88.
[5] Alom-Ruiz SP, Anilkumar N, Shah AM. Reactive oxygen species and endothelial activation. Antioxid Redox Signal 2008;10:1089–100.
[6] Davda J, Labhasetwar V. Characterization of nanoparticle uptake by endothelial cells. Int J Pharm 2002;233:51–9.
[7] Napierska D, Thomassen LC, Rabolli V, Lison D, Gonzalez L, Kirsch-Volders M, et al. Size-dependent cytotoxicity of monodisperse silica nanoparticles in human endothelial cells. Small 2009;5:846–53.
[8] Peters K, Unger RE, Kirkpatrick CJ, Gatti AM, Monari E. Effects of nano-scaled particles on endothelial cell function in vitro: studies on viability, proliferation and inflammation. J Mater Sci Mater Med 2004;15:321–5.
[9] Lin W, Huang YW, Zhou XD, Ma Y. In vitro toxicity of silica nanoparticles in human lung cancer cells. Toxicol Appl Pharmacol 2006;217:252–9.
[10] Park EJ, Park K. Oxidative stress and pro-inflammatory responses induced by silica nanoparticles in vivo and in vitro. Toxicol Lett 2009;184:18–25.
[11] Wang F, Gao F, Lan M, Yuan H, Huang Y, Liu J. Oxidative stress contributes to silica nanoparticle-induced cytotoxicity in human embryonic kidney cells. Toxicol In Vitro 2009;23:808–15.
[12] Eom HJ, Choi J. Oxidative stress of silica nanoparticles in human bronchial epithelial cell, Beas-2B. Toxicol In Vitro 2009;23:1326–32.
[13] Choi SJ, Oh JM, Choy JH. Toxicological effects of inorganic nanoparticles on human lung cancer A549 cells. J Inorg Biochem 2009;103:463–71.
[14] Davis RJ. Signal transduction by the JNK group of MAP kinases. Cell 2000;103:239–52.
[15] Wang XB, Gao HY, Hou BL, Huang J, Xi RG, Wu LJ. Nanoparticle realgar powders induce apoptosis in U937 cells through caspase MAPK and mitochondrial pathways. Arch Pharm Res 2007;30:653–8.
[16] Yu M, Mo Y, Wan R, Chien S, Zhang X, Zhang Q. Regulation of plasminogen activator inhibitor-1 expression in endothelial cells with exposure to metal nanoparticles. Toxicol Lett 2010;195:82–9.
[17] Li R, Ning Z, Cui J, Khalsa B, Ai L, Takabe W, et al. Ultrafine particles from diesel engines induce vascular oxidative stress via JNK activation. Free Radic Biol Med 2009;46:775–82.
[18] Ueda S, Masutani H, Nakamura H, Tanaka T, Ueno M, Yodoi J. Redox control of cell death. Antioxid Redox Signal 2002;4:405–14.
[19] Sun J, Ding T. p53 reaction to apoptosis induced by hydroxyapatite nanoparticles in rat macrophages. J Biomed Mater Res A 2009;88:673–9.
[20] Manna SK, Sarkar S, Barr J, Wise K, Barrera EV, Jejelowo O, et al. Single-walled carbon nanotube induces oxidative stress and activates nuclear transcription factor-kappaB in human keratinocytes. Nano Lett 2005;5:1676–84.
[21] Lipski AM, Pino CJ, Haselton FR, Chen IW, Shastri VP. The effect of silica nanoparticle-modified surfaces on cell morphology, cytoskeletal organization and function. Biomaterials 2008;29:3836–46.
[22] Teeguarden JG, Hinderliter PM, Orr G, Thrall BD, Pounds JG. Particokinetics in vitro: dosimetry considerations for in vitro nanoparticle toxicity assessments. Toxicol Sci 2007;95:300–12.
[23] Lison D, Thomassen LC, Rabolli V, Gonzalez L, Napierska D, Seo JW, et al. Nominal and effective dosimetry of silica nanoparticles in cytotoxicity assays. Toxicol Sci 2008;104:155–62.
[24] Jaffe EA, Nachman RL, Becker CG, Minick CR. Culture of human endothelial cells derived from umbilical veins. Identification by morphologic and immunologic criteria. J Clin Invest 1973;52:2745–56.
[25] Lu F, Wu SH, Hung Y, Mou CY. Size effect on cell uptake in well-suspended, uniform mesoporous silica nanoparticles. Small 2009;5:1408–13.
[26] Chen YH, Lin SJ, Ku HH, Shiao MS, Lin FY, Chen JW, et al. Salvianolic acid B attenuates VCAM-1 and ICAM-1 expression in TNF-alpha-treated human aortic endothelial cells. J Cell Biochem 2001;82:512–21.
[27] Vallet-Regi M, Balas F, Arcos D. Mesoporous materials for drug delivery. Angew Chem Int Ed Engl 2007;46:7548–58.
[28] Dimmeler S, Zeiher AM. Reactive oxygen species and vascular cell apoptosis in response to angiotensin II and pro-atherosclerotic factors. Regul Pept 2000;90:19–25.

[29] Li JM, Shah AM. Endothelial cell superoxide generation: regulation and relevance for cardiovascular pathophysiology. Am J Physiol Regul Integr Comp Physiol 2004;287:1014–30.
[30] Kim S, Choi JE, Choi J, Chung KH, Park K, Yi J, et al. Oxidative stress-dependent toxicity of silver nanoparticles in human hepatoma cells. Toxicol In Vitro 2009;23:1076–84.
[31] Leroueil PR, Hong S, Mecke A, Baker Jr JR, Orr BG, Banaszak Holl MM. Nanoparticle interaction with biological membranes: does nanotechnology present a Janus face? Acc Chem Res 2007;40:335–42.
[32] Gojova A, Guo B, Kota RS, Rutledge JC, Kennedy IM, Barakat AI. Induction of inflammation in vascular endothelial cells by metal oxide nanoparticles: effect of particle composition. Environ Health Perspect 2007;115:403–9.
[33] Xu F, Sun Y, Chen Y, Li R, Liu C, Zhang C, et al. Endothelial cell apoptosis is responsible for the formation of coronary thrombotic atherosclerotic plaques. Tohoku J Exp Med 2009;218:25–33.
[34] Pan Y, Leifert A, Ruau D, Neuss S, Bornemann J, Schmid G, et al. Gold nanoparticles of diameter 1.4 nm trigger necrosis by oxidative stress and mitochondrial damage. Small 2009;5:2067–76.
[35] Hsin YH, Chen CF, Huang S, Shih TS, Lai PS, Chueh PJ. The apoptotic effect of nanosilver is mediated by a ROS- and JNK-dependent mechanism involving the mitochondrial pathway in NIH3T3 cells. Toxicol Lett 2008;179:130–9.
[36] Yuan Y, Liu C, Qian J, Wang J, Zhang Y. Size-mediated cytotoxicity and apoptosis of hydroxyapatite nanoparticles in human hepatoma HepG2 cells. Biomaterials 2010;31:730–40.
[37] Martindale JL, Holbrook NJ. Cellular response to oxidative stress: signaling for suicide and survival. J Cell Physiol 2002;192(1):1–15.
[38] Simbula G, Columbano A, Ledda-Columbano GM, Sanna L, Deidda M, Diana A, et al. Increased ROS generation and p53 activation in alpha-lipoic acid-induced apoptosis of hepatoma cells. Apoptosis 2007;12:113–23.
[39] Fuchs SY, Adler V, Pincus MR, Ronai Z. MEKK1/JNK signaling stabilizes and activates p53. Proc Natl Acad Sci U S A 1998;95:10541–6.
[40] Schanen BC, Karakoti AS, Seal S, Drake 3rd DR, Warren WL, Self WT. Exposure to titanium dioxide nanomaterials provokes inflammation of an in vitro human immune construct. ACS Nano 2009;3:2523–32.
[41] Oesterling E, Chopra N, Gavalas V, Arzuaga X, Lim EJ, Sultana R, et al. Alumina nanoparticles induce expression of endothelial cell adhesion molecules. Toxicol Lett 2008;178:160–6.
[42] Moghimi SM, Hunter AC, Murray JC. Nanomedicine: current status and future prospects. FASEB J 2005;19:311–30.
[43] Baeuerle PA, Henkel T. Function and activation of NF-kappa B in the immune system. Annu Rev Immunol 1994;12:141–79.
[44] Endemann DH, Schiffrin EL. Endothelial dysfunction. J Am Soc Nephrol 2004;15:1983–92.